FINAL REPORT

FOR CRADA NO. C-06-14

BETWEEN

BROOKHAVEN SCIENCE ASSOCIATES

AND

RADIATION MONITORING DEVICES, INC.

Project Entitled: Fast Dense Low cost Scintillator for Nuclear Physics

Brookhaven PI: Craig Woody

Submitted by: Michael J. Furey
Manager, Research Partnerships
Brookhaven National Laboratory

DISCLAIMER

FINAL REPORT

FOR CRADA NO. C-06-14

BETWEEN

BROOKHAVEN SCIENCE ASSOCIATES

AND

RADIAION MONITORING DEVICES, INC.

Project Entitled: Fast Dense Low cost Scintillator for Nuclear Physics

Brookhaven PI: Craig Woody

Submitted by: Michael J. Furey
Manager, Research Partnerships
Brookhaven National Laboratory

DISCLAIMER

TABLE OF CONTENTS

1. BACKGROUND

Inorganic scintillators are one of the most common gamma ray sensors at present and are widely used in existing nuclear and particle physics experiments. These detectors are also expected to be a very important component of future nuclear physics experiments including those being planned for the Rare Isotope Accelerator [1]. In addition to nuclear and particle physics, scintillation spectrometers are routinely used in nuclear nonproliferation, medical imaging, environmental monitoring, nondestructive testing, and geological exploration [2].

The performance of the systems used in these applications is often limited by the properties of scintillation detectors available at present. Important requirements for the scintillation crystals used in these applications include high light output, high gamma-ray attenuation, fast response, high energy and timing resolution, low cost, and good proportionality [3,4,5]. Moreover, since the highly energetic gamma photons penetrate up to a centimeter or more into the bulk of even the densest scintillators, it is also essential that the scintillator be highly transparent. All these requirements cannot be met by any of the commercially available scintillators. Also, the high cost associated with the growth of good quality, uniform single crystals (especially for materials that melt at very high temperature such as LSO and GSO) is a major limitation.

Recently, RMD reported on a new class of materials, the cerium-doped hafnates, which were explored during the completed Phase II research project for particle physics applications. In particular, $SrHfO_3$:Ce, $BaHfO_3$:Ce and $Lu_2Hf_2O_7$:Ce have excellent gamma ray stopping efficiency due to their high density (7.7, 8.5, and 9.4 g/cm^3, respectively) and show a light output under X-ray excitation that is much higher than that of BGO. For example, the light output of $BaHfO_3$:Ce was measured to be 28,000 photons/MeV, which is 3½ times higher than that of BGO, whereas the light output of $SrHfO_3$:Ce was recorded to be as high as 45,000 photons/MeV, 5½ times higher than that of BGO. The light yield of $Lu_2Hf_2O_7$:Ce was of the same order as that of BGO. $SrHfO_3$:Ce, $BaHfO_3$:Ce and $Lu_2Hf_2O_7$:Ce were found to have a peak emission wavelength of approximately 400 nm and a fast scintillation decay of about 10 - 20 ns with a rise time of approximately 200 ps. In addition, their nearly isotropic optical properties allow for the fabrication of fully transparent optical ceramics (TOC), providing a reliable and low cost alternative to single crystal growth. Clearly, these results indicate that $SrHfO_3$:Ce, $BaHfO_3$:Ce and $Lu_2Hf_2O_7$:Ce are unique materials that combine a high density with good light output and a fast scintillation decay, and therefore, have the potential to offer a unique alternative to traditional crystal scintillators such as BGO, LSO and GSO, with potentially better performance, greater reproducibility, and significantly lower cost.

2. TECHNICAL OBJECTIVES

The Phase II effort was built on the success of Phase I, with the initial focus on further optimization of the optical ceramic technology for the cerium-doped hafnate scintillators, particularly $SrHfO_3$:Ce, $BaHfO_3$:Ce and $Lu_2Hf_2O_7$:Ce. The preparation of transparent optical ceramics with improved transparency has been a crucial aspect of this work. In our experience with another optical ceramic, Lu_2O_3, we found that a narrow grain size distribution, reduced porosity, and elimination of light-scattering second phases are very important for producing ceramic samples with a high degree of transparency. Hence, the first step in our ceramic preparation process was focused on producing powders of the candidate hafnates with as narrow a particle size distribution as reasonably possible, and with absolute sizes and morphology tailored to the consolidation process so as to maximize the feasibility of achieving full density. Consequently we explored a number of different techniques to fabricate the requisite powders, ultimately settling on two, one for each consolidation process. Powders were fabricated both in-house and by commercial sources, and each played a major role in our study.

Two different consolidation processes were studied in this program, mechanical hot pressing and sintering followed by hot isostatic pressing (conventionally termed *sinter-HIPing*). Each technique was extensively studied through systematic variation of densification parameters in an effort to define the conditions that will produce optimal specimens. The resulting hafnate ceramic specimens were extensively characterized and compared with high quality LSO and BGO single crystals, including measurement of light output, decay time, emission spectrum, and energy and timing resolution, with particular attention to their potential performance in nuclear and particle physics applications. The possibility of using these new scintillators in other potential applications such as X-ray computed tomography was also investigated during the Phase II research project.

This effort has been a joint venture between RMD, Inc. and ALEM Associates, both of which have extensive experience in scintillators, gamma ray detectors and nuclear instruments. A major collaborator in this project was Dr. Vinod Sarin at Boston University's Department of Manufacturing Engineering, who was responsible for the hot pressing of the hafnate powders to produce optical ceramics. Also participating in the ceramic fabrication effort as consultant was Dr. William H. Rhodes, who is one of the foremost authorities on powder consolidation and ceramics. Other participants included Dr. Craig Woody at the Brookhaven National Laboratory, an expert in scintillators and detectors for nuclear and particle physics applications, who was to perform optical and radiation hardness measurements on suitable specimens; Dr. William Moses at Lawrence Berkeley National Laboratory, to provide support in scintillator characterization as needed; and Dr. Partha Chowdhury at the University of Massachusetts (U-Mass, Lowell) and Dr. C.J. Lister at Argonne National Laboratory, to evaluate appropriate scintillator specimens s for nuclear physics applications.

3. TECHNICAL PROGRESS

3.1. OVERVIEW

This program began with three candidate materials, $SrHfO_3$, $BaHfO_3$, and $Lu_2Hf_2O_7$. In Phase I we successfully demonstrated that all three could be fabricated in the form of transparent optical ceramics, with densities and scintillation capabilities appropriate for use in nuclear physics applications. Each, however, displayed its unique combination of advantages and drawbacks. Lutetium hafnate ceramics, for example, show the best transparency of the three, but the lowest light output. This low light yield (see **Figure 1**) is probably related to the crystal structure of the material, a disordered defect cubic pyrochlore in which the cation sites are randomly occupied by either Lu^{3+} or Hf^{4+} ions [6]. While the Ce activator could enter the lattice substitutionally in either site, the ionic radius of Ce^{3+} is considerably larger than that of Lu^{3+}, while Ce^{4+} fits quite nicely into the Hf site. Thus the great preponderance of the cerium goes in as a tetrapositive ion, which happens not to emit at all, rather than as the strongly emitting 3+ ion needed for scintillation. We attempted to stabilize the desired tripositive state by codoping with fluorine ions, but we were not successful in improving the light output.

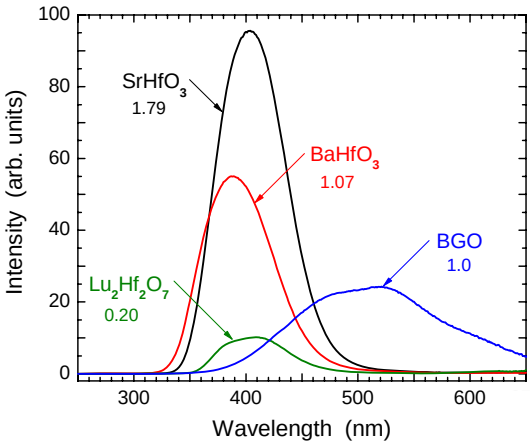

Figure 1. Radioluminescence spectra of the three hafnate ceramics and comparison with BGO. Numbers below ID tags indicate total (spectrally integrated) light relative to BGO.

Barium hafnate showed different problems. Here the size of the lattice site was not the problem since Ba^{2+} is actually larger than Ce^{3+} and its lattice site will easily accommodate this dopant in the 3+ state. Consequently here we needed only to avoid substantial exposure to oxidizing conditions and to add a corresponding amount of Al^{3+} as a codoping substituent for Hf^{4+} to provide charge balance. Unfortunately, barium hafnate posed a more subtle problem: As it turns

out, the vapor pressure of barium oxide at the temperatures required for hot pressing to full density is high enough to lead to substantial barium deficit, particularly at higher processing temperatures. In principle, this could be addressed by providing a suitable excess of barium content in the starting powder, but this quantity would necessarily vary depending on the temperature and duration of the consolidation step, making it extremely difficult to define optimum consolidation conditions. Thus, even though we were able to fabricate $BaHfO_3$:Ce ceramics of adequate transparency (this cubic material does, after all, have full optical isotropy), its scintillation light yield was substantially less than that of its strontium counterpart (again see **Figure 1**), and remained so despite numerous variations in consolidation conditions or post-treatment. We even explored the potential of mixed crystals (that is, introducing into the barium hafnate lattice as much strontium as it could accommodate without losing its cubic structure), but to no avail. The details of these efforts have already been presented in an earlier report.

This left us with strontium hafnate as the most promising candidate material for this program. The material is by no means ideal: For one thing, it poses the same vapor pressure issue as its barium counterpart, but at a far more tractable magnitude. Also, its structure is orthorhombic rather than cubic, albeit with relatively small refractive index differences. But the material has two compelling factors in its favor: It can indeed be consolidated into fully dense transparent optical ceramics of sufficiently high quality for scintillator application, as we have already demonstrated; and it consistently displays the highest light yield. Consequently, we decided that the most prudent course of action for the latter part of the program was to concentrate our effort on the strontium hafnate material, which we judged would give us the best chance of reaching our goal. We discuss this in more detail below.

3.2. Powder Development and Consolidation

An accepted truth in ceramic technology is that the product is only as good as the powder from which it is made. In order to manufacture transparent optical ceramic (TOC) scintillators, it is crucial to have good precursor powder with the right composition. Moreover, the particle size of the powder must be appropriate to the specific technology used for consolidation to full density. Consequently, much attention was focused on powder optimization, an iterative development effort in which the results of the consolidation experiments provided the primary guidance. Moreover, since we were applying two different powder densification technologies, hot pressing and sinter-HIPing, it is not surprising that the optimal requirements for starting powders were found to differ substantially. In particular, sinter-HIPing requires smaller particle size than hot pressing, in order to enable achievement of closed porosity at lower temperatures and without excessive grain growth. Since we have already presented the details of the powder development effort in previous reports, we present in the following only a brief summary of the results.

3.2.1. Solid State Synthesis

The simplest technique for powder synthesis was by means of *solid-state reaction*. This term is often used to describe interactions where neither a solvent medium nor controlled vapor-phase interactions are utilized. Materials are prepared using furnaces, which allow reaction between chemicals to be conducted at temperatures up to 2000°C. For the synthesis of strontium hafnate, we used the solid-state reaction between $SrCO_3$ and HfO_2 to produce $SrHfO_3$:Ce. Here we used stoichiometric amounts of $SrCO_3$ [Alfa, 99.99%] and HfO_2 [Cerac, 99.95%]. The two compounds were mixed and milled for several hours in isopropanol [Alfa, ACS] using zirconia media. After drying, a small amount of $Ce(NO_3)_3{\cdot}6H_2O$ [Aldrich, 99.999%], $Al(NO_3)_3{\cdot}9H_2O$ [Aldrich, 99.997%], and a molar excess of oxalic acid dihydrate [Alfa, ACS] was added. The aluminum was added as a co-dopant to compensate for the charge mismatch that occurs when Ce^{3+} enters a lattice site that would otherwise be occupied by Sr^{2+}. By substituting for Hf^{4+}, the Al^{3+} corrects the charge imbalance that would otherwise allow the insertion of Ce^{4+} into Hf^{4+} lattice sites, with adverse impact on the scintillation properties of the ceramic. The mixture was milled overnight while allowing for the

evaporation of CO_2, which is released during the reaction between the oxalic acid and the metal carbonates. The resulting slurry was dried overnight, calcined in air at 1200°C for 4 hours and calcined in forming gas (95% N_2, 5% H_2) at 1200°C for 4 hours. Finally, the powder was sieved using a -100 mesh nylon screen.

The smallest average particle size that we were able to achieve through such synthesis was on the order of half a micron (**Figure 2**). While this was too high for the sinter-HIP process, our in-house powder did ultimately give very good results by hot pressing, as will be seen later.

Figure 2. SEM micrograph of strontium hafnate powder synthesized by solid-state reaction. The average particle size is ~600 nm, but with some larger (2-2.5 μm) agglomerates.

Unfortunately, our results with powder developed by an external vendor, TransTech Corp. (Adamstown, MD), were nowhere nearly as successful. With an eye toward eventual commercialization, we had chosen TransTech as a potential supplier on the basis of their extensive experience with chemically similar materials, such as strontium titanate. Indeed their powders showed good physical characteristics, with a particle size on the order of 0.5 – 2 μm and good morphology. However, both of their hafnate powders (strontium as well as barium) simply did not produce adequate specimens by means of hot pressing, with sample after sample showing evidence of departure from stoichiometry as well as a persistent intergranular glassy phase containing high levels of silicon and carbon. The presence of such foreign phases proved to be an insurmountable barrier to the achievement of transparency with the TransTech powders, and this effort was ultimately abandoned.

3.2.2. Sol-Gel Synthesis

We did, however, also explore a wet chemical technique, namely the *sol-gel process*. This starts with a solution ("sol") of inorganic/organic precursors, which is then subjected to chemical treatment to produce an integrated network ("gel"). Typically, the precursors are metal alkoxides, which undergo hydrolysis and condensation reactions to form a system composed of solid particles dispersed in the solvent. When dried, the gel transforms into a powder having a relatively small particle size (on the order of 1 micron), with fairly narrow size distribution.

For this program, we synthesized strontium hafnate doped with trivalent cerium by using stoichiometric amounts of $Sr(OC_3H_7)_2$ [Strem, >95%], $Hf(OC_2H_5)_4$ [Gelest, >95%], a small amount of $Ce(NO_3)_3{\cdot}6H_2O$ [Aldrich, 99.999%], and $Al(NO_3)_3{\cdot}9H_2O$ [Aldrich, 99.997%]. The starting materials were dissolved in methoxyethanol to obtain the sol. The elaboration proceeded by adding a few hundred milliliters of de-ionized water to the sol which immediately yielded a thick gel of polymer chains of strontium hafnate. Subsequently, the gel was dried at approximately 100ºC for about 24 hours to remove water and the remainder of the methoxyethanol solvent. Next, the gel was calcined in air at 1000ºC for about 6 hours to burn off residual organic compounds, and calcined in forming gas (95% N_2, 5% H_2) at 1200ºC for about 4 hours. Finally, the powder was milled in isopropanol using yttria-stabilized zirconia media for about 8 hours, dried, and sieved using a -100 mesh nylon screen.

Size analysis of this powder indicated that a relatively large particle size of about one micron was obtained after calcination. Repeated calcining studies showed that due to the nature of the sol-gel process, the formation of $SrHfO_3$ particles from the sol-gel network proceeded quite rapidly and submicron particles could not be obtained. Consequently, this technique was not deemed suitable to provide submicron $SrHfO_3$:Ce powders for use in sinter-HIPing. Moreover, while the sol-gel pow-

ders would indeed be suitable for hot pressing, we did not feel that they provided any profound advantage over solid state reaction that would justify the high cost of the starting materials (metal alkoxides) particularly with regard to the ultimate commercial manufacture of $SrHfO_3$:Ce TOC.

3.2.3. Combustion Synthesis

Unfortunately (as described above), the solid-state reaction approach proved unsuitable to produce the submicron powder needed for sinter-HIPing. The need for a high calcination temperature (~1200°C) to obtain phase-pure hafnates invariably caused an unacceptable increase in particle size. One approach to resolve this conflict utilizes *combustion synthesis*. This process, which is characterized by fast heating rates and short reaction times [7], can provide finely divided powder at temperatures significantly less than those used in equivalent solid state reactions. The process involves an exothermic reaction between metal nitrates and a fuel such as citric acid, EDTA, or carbohydrazide.

To prepare $SrHfO_3$:Ce powder by the combustion approach, we used $Sr(NO_3)_2$ [Alfa, 99.95%], $Ce(NO_3)_3{\cdot}6H_2O$ [Aldrich, 99.999%], $HfO(NO_3)_2{\cdot}2H_2O$ [NOAH, 99.95%], with citric acid or carbohydrazide as fuel. This produced powder of the appropriate stoichiometry and phase purity, with a particle size distribution shown in **Figure 3**. Here we see an average particle size of about 170 nm, considerably finer than the approximately half micron that we obtained with solid state synthesis. Note the single-mode nature of the distribution, with no evidence of agglomerates.

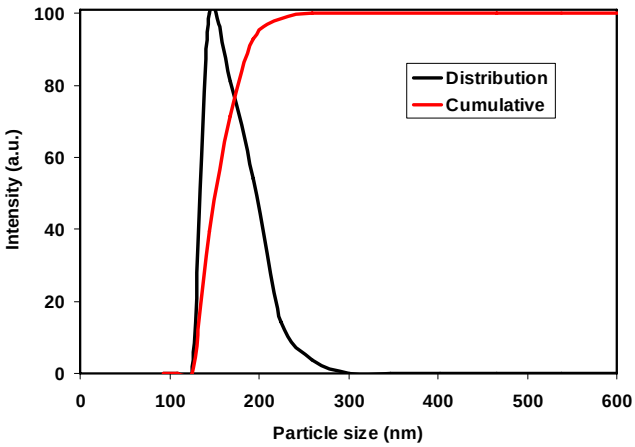

Figure 3. Particle size distribution of $SrHfO_3$:Ce powder synthesized by the combustion-synthesis method.

Unfortunately, however, the extremely exothermic reaction gave us great difficulty in controlling the synthesis and in most cases only a fraction of the powder could be recovered. Also, the stress to the laboratory equipment used was unacceptably high and in one case resulted in the destruction of the reactor vessel. Consequently, we rejected this method to produce $SrHfO_3$:Ce nanopowder; although the technique in theory could provide high-quality starting material for a sinter-HIP approach to the manufacture of $SrHfO_3$:Ce TOCs, we felt that the following technique was far more appropriate.

3.2.4. Flame-Spray Pyrolysis

The core technology of this effort consists of specially controlled *Liquid Phase Flame Spray Pyrolysis* (L-FSP), which has been successfully used to prepare a wide variety of mixed metal oxide nanopowders with controlled and optimized composition, purity, phase, morphology, and nanostructure. Although also a combustion technique, this approach differs from the previous one in that the combustion is induced rather than intrinsic. Here we have organometallic precursors dissolved in a combustible organic solvent and sprayed as a fine mist into a reaction chamber where it ignites. Thus the reaction temperature is defined not by the kinetics of the chemical reaction but rather by the dynamic steady state conditions in the flame as established by the pressures, concentrations and feed rates of the reactants. This makes the conditions far more controllable, and the product far more predictable, than in the previous case. Since the synthesis of nanoparticulate powders involves highly specialized experience and technology, this effort was carried out by a commercial vendor of such powder, Nanocerox Inc. (Ann Arbor, MI), which is an established leader in the field.

The strategy of flame synthesis in general is well known and has been used industrially for the production of carbon black for well over 100 years [8]. The hydrolysis of volatile precursors such as

$SiCl_4$ and $TiCl_4$ are used today to produce kiloton quantities of high surface area SiO_2 and TiO_2 powders [9]. The unique variation practiced by Nanocerox, so-called *Liquid Phase Flame Spray Pyrolysis* (L-FSP), relies on controlled combustion of stoichiometric mixtures of soluble metal precursors dissolved in a flammable carrier solvent. It has been patented by the University of Michigan, where the core concepts were originally developed, and licensed exclusively to Nanocerox [10]. After several years of development, the original technology has been refined and expanded in scope, such that the custom synthesis of a large catalog of mixed metal oxide nanopowders is now routine [11].

Hafnates, however, were not a part of Nanocerox's product line, necessitating a significant development effort to identify the proper fabrication conditions. Although this was ultimately quite successful (see **Figure 4**), it did limit the time we had available for a concerted study of the sinter-HIPed ceramic itself. Nevertheless, we were able to amass a substantial body of information on these materials, details of which are presented in subsequent sections.

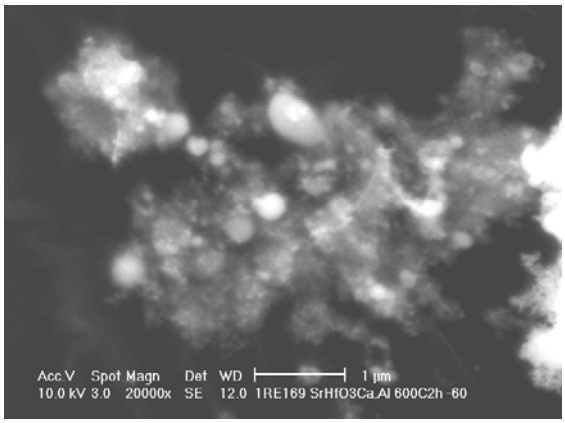

Figure 4. SEM micrograph of strontium hafnate powder synthesized by Nanocerox by means of Liquid Phase Flame Spray Pyrolysis (L-FSP). The particles are spherical, with an average size of ~40 nm.

3.3. CERAMIC FABRICATION

3.3.1. Hot Press Consolidation Process

As discussed in **Section 3.2**, all powders used in the hot pressing experiments were obtained via solid state synthesis. The single-phase nature of these powders was confirmed by XRD, although these measurements could not preclude the presence of small amounts (up to ~1%) of foreign-phase contamination, which could be detected only by microscopic examination of consolidated disks. While this should not substantially affect scintillation performance, the impact on transparency can be substantial, and will have to be addressed.

The hot pressing process proceeded as follows: First, a predetermined volume of powder was charged into a graphite die whose walls were coated with boron nitride. The die was placed in the hot press chamber and the system evacuated to below 100 mtorr. Mechanical pressure was applied through a graphite piston as the temperature was raised. The ceramics were hot pressed at different temperatures and held at each temperature for 2 hours while subjected to 8,800 psi uniaxial pressure. After hot pressing, the samples were polished before characterization.

3.3.2. Sinter-HIP Consolidation Process

For sinter-HIP consolidation, we used only the sub-micron powder supplied by Nanocerox. This powder was subjected to the same pre-consolidation screening by XRD as had been applied to the product synthesized by solid state reaction. Here, however, the diffraction patterns were less satisfactory, with broad lines suggestive of a highly disordered or even amorphous network, and indications of incomplete reaction between the constituent oxides. While calcination at z00 C could largely correct this problem, we found that it made little difference in the final (consolidated) compact.

Unlike hot pressing, which directly transforms loose powder into fully dense ceramic, sinter-HIPing has at least three distinct stages. To begin, the starting powder is compacted into a self-cohesive mass (at or near room temperature) by external force alone, applied first by a mechanical press and then by cold isostatic pressing. This forces the individual powder particles into as close proximity as possible, so as to maximize the effectiveness of the sintering step to follow At this point the so-called green body has a density some 55-60% of that of the single crystal.

In the next step this green body is placed in a furnace (in vacuum or diffusible gas atmosphere) and slowly raised to a temperature high enough (typically y000 C, some a00 C below the melting

point) for material diffusion to take place between neighboring particles, at a rate sufficient to seal off all residual porosity and isolate it from the external environment. Now the density must be at least 92% of the fully dense crystalline phase; any lesser value is taken as an indication that closed porosity has not been achieved, and that subsequent HIPing will not succeed.

In the last step, the successfully sintered compact is placed into a hot isostatic press, where it is again heated to a temperature about the same as (or perhaps a bit more than) that at which it had been sintered, but now while immersed in a nondiffusible gas (typically argon or nitrogen) that is pressurized on the order of 50 ksi. Holding the specimen under these conditions drives the residual pores to close or diffuse out of the bulk of the compact, bringing it to essentially the same density as that of the single crystal (>99.5%), but in the form of a pore-free polycrystalline mass. Finally (as before), the specimens were polished prior to evaluation.

3.4. Evaluation of Hot-Pressed Strontium Hafnate

The various hafnate specimens were subjected to a comprehensive series of characterization measurements. Many of the $BaHfO_3$ and $Lu_2Hf_2O_7$ results have been presented in previous reports and will not be repeated here. Both of these materials exhibited their own unique attractions, but, for reasons discussed earlier, ultimately fell by the wayside. Consequently the subsequent discussion will focus on the strontium hafnate material, which we deemed to have the greatest potential as a scintillator for nuclear physics applications. Each type of relevant measurement will be discussed in turn.

3.4.1. Chemical Fidelity

Prior to any consolidation experiments, a primary consideration is the chemical integrity of the material. As we had noted earlier, we had a great deal of concern regarding whether the non-negligible vapor pressure of SrO at processing temperatures could be a factor in driving the material off stoichiometry during the synthesis or consolidation processes. Consequently, we ran a series of tests on powders specifically prepared with various proportions of the constituent oxides, SrO and HfO_2. These powders were then calcined at temperatures ranging as high at 1200 C, followed by chemical analysis by ICP (Dirats Laboratories, Westfield MA) and crystallographic analysis by XRD on a Bruker AXS diffractometer at Boston University.

Table 1. ICP Analysis of Strontium Hafnate Powder

Nominal Composition	ICP (mol%)				(Sr+Ce)/(Hf+Al)
	Sr	Hf †	Ce	Al	
$Sr_{0.995}Ce_{0.005}Hf_{0.995}Al_{0.005}O_3$	0.318	0.316	0.00105	0.00196	1.003
$Sr_{1.095}Ce_{0.005}Hf_{0.995}Al_{0.005}O_3$	0.342	0.304	0.00070	0.00451	1.111

† *excluding ZrO_2 impurities*

Table 1 shows the results of ICP analysis on two different $SrHfO_3$:Ce powder batches made with 0% and 10% excess strontium oxide (SrO), respectively. Here we see that the initial proportions of the constituents, with or without excess SrO, are preserved in the calcined $SrHfO_3$:Ce powders. Thus it would appear that no significant amount of SrO escapes during calcination, even at temperatures as high as 1200°C.

X-ray diffraction (XRD) spectra of $SrHfO_3$:Ce powders synthesized with different amounts of SrO are shown in **Figure 5**. The standard ICDD XRD pattern of orthorhombic $SrHfO_3$ (PDF card No. 01-089-5606) is also shown, as reference. All diffraction patterns of $SrHfO_3$:Ce powders confirm their orthorhombic structure regardless of any excess amount of SrO. These observations are in contrast with those of Villanueva-Ibañez *et al*. [12]

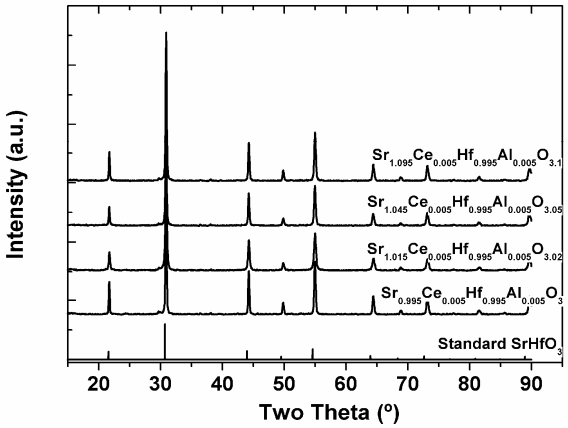

Figure 5. X-ray diffraction spectra of various strontium hafnate powders.

where monoclinic HfO_2 impurities were observed for $0.66 \leq Sr/Hf \leq 1.04$. We attribute the presence of HfO_2 in their powders to their inhomogeneous preparation by the sol-gel method.

Note that XRD measurements do not detect free SrO in the $SrHfO_3$:Ce powders, even when ICP data clearly indicate the presence of excess Sr over Hf. A possible explanation would be the formation of a solid solution of SrO and $SrHfO_3$ in the Sr-rich range ($Sr/Hf > 1$) of the HfO_2-SrO phase diagram [13]. However, at the moment we cannot confirm this hypothesis.

3.4.2. Phase Fidelity

Although our concerns about compositional drift have been largely allayed, this does not hold true for the crystallographic structure as well. Indeed (as mentioned previously), $SrHfO_3$ exhibits several phase changes in the solid [14]. Consequently, we performed both Differential Thermal Analysis (DTA) on powders and Thermal Expansion measurements on hot-pressed ceramics, with the intent to quantify these effects. DTA measurements were performed using a TA Instruments SDT Q600 using an alumina reference in flowing argon. Approximately 35 mg of $SrHfO_3$ powder was measured. The furnace temperature was increased at a rate of 3°C/min. up to 1450°C, held for 2 hours and subsequently decreased at a rate of 5°C/min. The software provided with the Q600 was used to calculate the heat flow. Thermal Expansion measurements were performed at Netzsch Instruments (Burlington MA) using a DIL 402C vacuum-tight, horizontal pushrod dilatometer. Ceramic samples were mounted on an alumina holder and heated at a rate of 5°C/min. The thermal expansion was measured from 100 to 1400°C, using sapphire as calibration standard.

Heat flow measurements as function of temperature, shown in **Figure 6**, clearly indicate the presence of several transitions in the temperature range 500 - 1400°C. Kennedy and Howard [14] concluded that $SrHfO_3$ can exist in four phases, two orthorhombic, one tetragonal and one cubic. At room temperature, the phase of $SrHfO_3$ is orthorhombic (P*nma*) which rearranges into a second orthorhombic phase at 500±100 C (C*mcm*). Subsequently, the material transforms into a tetragonal phase (I*4/mcm*) at 675±75 C, and finally converts into the cubic (P*m3m*) structure at 1105±25 C; *i.e.*,

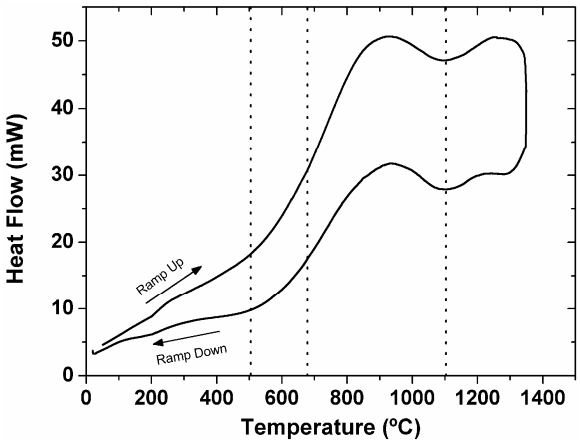

Figure 6. Differential thermal analysis (DTA) of $SrHfO_3$:Ce powder.

$$Pnma \xrightarrow{673-873\,K} Cmcm \xrightarrow{873-1023\,K} I4/mcm \xrightarrow{1353-1403\,K} Pm\bar{3}m\,.$$

These transition temperatures are indicated in **Figure 6** by dotted lines. The most evident transition is that from I*4/mcm* to P*m3m*, corresponding to a local minimum in the heat flow measurements at ~1100°C. The transitions from P*nma* to C*mcm* and from C*mcm* to I*4/mcm* are not readily apparent. From the lattice constants, we derived the approximate densities of the various $SrHfO_3$ phases (see **Table 2)**. Overall, the density decrease from P*nma* to P*m3m* is about 3%.

Table 2. Calculated densities of the $SrHfO_3$ phases

Structure	Space group	Cell volume (Å)	Z	Density (g/cm^3)	Density Change
Orthorhombic	P*nma*	269.70	4	7.736	
Orthorhombic	C*mcm*	548.09	8	7.613	-1.59%
Tetragonal	I*4/mcm*	275.37	4	7.577	-1.12%
Cubic	P*m3̄m*	69.62	1	7.492	-0.47%

The thermal expansion behavior of a $SrHfO_3$:Ce ceramic is shown in **Figure 7**. Note that the dotted curve describing the mean thermal expansion coefficient (α) shows sudden changes in slope at about 670ºC, 1060ºC and 1350ºC. The first two can be related to the phase change from C*mcm* to

I*4/mcm*, and from I*4/mcm* to P$m\bar{3}m$, respectively. Even without these irregularities the curve is decidedly nonlinear, rising significantly with temperature at the lower end of the range but leveling off at about $10\times10^{-6}K^{-1}$ by ~1100°C. The solid curve showing the total linear expansion (averaged over all grain orientations) is much smoother, with barely perceptible jogs or slope changes over the entire temperature range.

Yamanaka *et al*. [15] obtained similar results for the density and thermal expansion coefficient. In addition, the Young's modulus and Vickers hardness of a sintered sample was found to be 219.8 and 9.31 GPa, respectively, making $SrHfO_3$:Ce a somewhat harder but equally stiff material compared to other perovskites such as $SrZrO_3$ and $SrTiO_3$.

The implications of the observed phase transitions for the achievement of a high degree of transparency in the ceramic are not immediately apparent. What is important here is not the magnitude of the average bulk properties but the extent to which they vary with crystallographic orientation. Although the transitions are an undesirable complication, the density changes and irregularities in thermal expansion are small enough to minimize the chances of self-destruction through thermal stress.

3.4.3. Microstructure of the Ceramic

The next thing we examined was the influence of chemical composition on the microstructure of the $SrHfO_3$ ceramic. For this we fabricated specimens from two batches of $SrHfO_3$ powder containing 0.5 mol percent each of Ce^{3+} and Al^{3+}. The only difference was that one was stoichiometric with regard to SrO and HfO_2 (*i.e.,* in 1:1 ratio), while the other had a 5 mol percent excess of SrO. The resulting microstructures are shown in **Figures 8** and **9**, respectively. Here each grain is seen in its own distinct shade of gray, presumably because their differences in orientation affects electron channeling and hence signal intensity*. The digits superimposed on each figure identify five points in each specimen that were chosen for microprobe measurements, four within well-defined grains and one

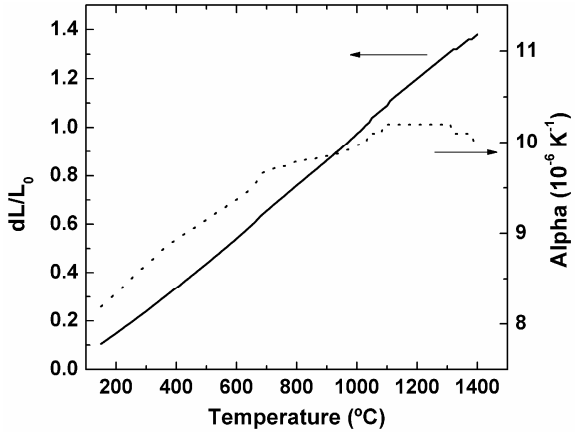

Figure 7. Thermal expansion of $SrHfO_3$:Ce ceramic. The solid and dotted lines represent the linear expansion and change in expansion coefficient (alpha), respectively.

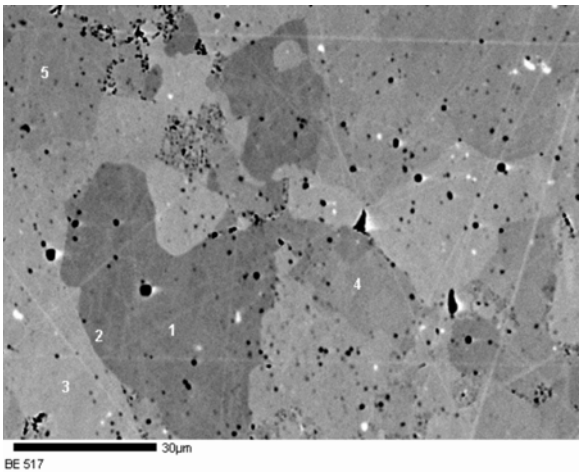

Figure 8. Microprobe photograph of strontium hafnate ceramic made from stoichiometric powder (*i.e.*, $Sr_{0.995}Ce_{0.005}Hf_{0.995}Al_{0.005}O_3$).

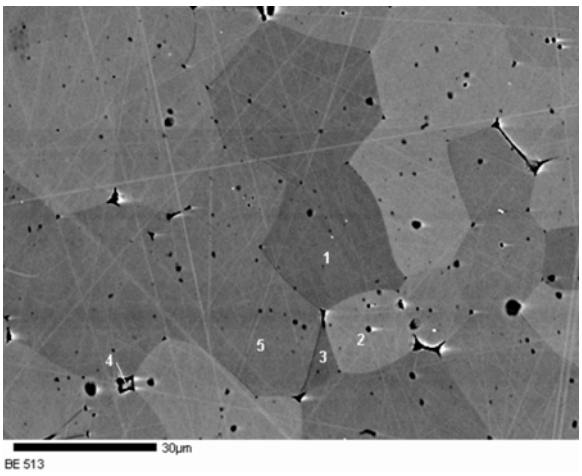

Figure 9. Microprobe photograph of strontium hafnate ceramic made from powder containing 5% excess SrO (*i.e.*, $Sr_{1.045}Ce_{0.005}Hf_{0.995}Al_{0.005}O_{3.05}$).

* The various levels of gray cannot be due to atomic number backscattering differences, since the grains have virtually identical chemical composition (See **Table 3**). Also note high incidence of trapped porosity; this indicates overly rapid grain growth, which was subsequently corrected (see **Figure 10**).

at a grain boundary or triple point. As shown in **Table 3**, each of the grains has an elemental content in good agreement with the nominal composition of the bulk, but with one key exception: almost none of the grains contains any detectable aluminum. In contrast, the phase at the triple point is not only deficient in hafnium and cerium, but also contains virtually all of the aluminum, at a level more than two orders of magnitude greater than theoretical. Moreover, this is not an isolated occurrence, but was found everywhere measurements were made, over the entire surface of the ceramic specimens. It appears that Al^{3+}, which is essential for charge compensation of Ce^{3+} [16], is either strenuously expelled from the host lattice, or is never accepted in the first place. Either way, its absence annuls the purpose of charge compensation, namely to prevent the formation of Ce^{4+} located at Hf^{4+} lattice sites, with adverse impact on the emission of the ceramic. Note that both specimens have the same Sr content regardless of whether excess was present in the powder. Each grain appears to be homogeneous, with no secondary phase. Since no signs of strontium depletion had been seen in the calcined powder (see **Section 3.4.1**), we assume that it was lost during hot pressing.

Table 3. Elemental content at designated locations in $SrHfO_3$ ceramic

Excess Sr	Label	Composition (weight percent)				
		Sr	Ce	Hf	Al	O
none (Figure 8)	*nominal**	*27.80*	*0.22*	*56.63*	*0.04*	*15.31*
	1	27.28	0.21	56.33	0.00	16.17
	2	27.22	0.23	56.54	0.02	15.99
	3	27.28	0.30	56.10	0.00	16.32
	4	27.74	0.24	56.23	0.01	15.78
	5	27.29	0.22	56.26	0.00	16.23
5% (Figure 9)	*nominal**	*28.72*	*0.22*	*56.63*	*0.04*	*15.31*
	1	27.58	0.21	57.06	0.00	15.15
	2	27.87	0.19	56.65	0.00	15.30
	3	27.47	0.21	56.98	0.00	15.34
	4	26.17	0.07	45.66	**6.19**	21.91
	5	27.59	0.16	56.95	0.00	15.30

* *i.e.*, according to formulas stated in the respective figures.

We also studied the dependence of grain size on hot-press temperature. **Figure 10** shows SEM micrographs of strontium hafnate ceramics hot-pressed at 1500, 1600, and 1700ºC. At 1500°C the grains are approximately 1 μm and equiaxed. However, at 1600°C the grain size distribution is decidedly bimodal, with the large grains having straight sides. This is usually an indication that grain growth was controlled by a grain boundary liquid phase. Since SrO is lost during hot pressing and Al_2O_3 segregates at grain boundaries, formation of a liquid phase is probable. By 1700°C the small grains are no longer present, once again revealing a near equiaxed structure, albeit with grains some two orders of magnitude larger.

3.4.4. Optical Properties of the Ceramic

To evaluate the transparency of $SrHfO_3$:Ce ceramics, visual inspection using a light box and measurements of the angular distribution of scattered light were performed. Conventionally, a ce-

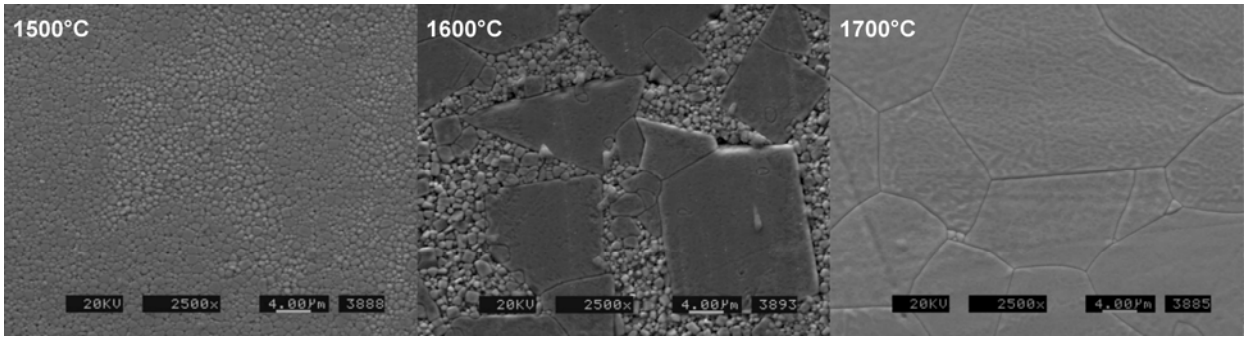

Figure 10. Grain size of $SrHfO_3$ ceramic as function of hot pressing temperature. Magnification 2500×.

ramic sample is placed directly onto a back-lit pattern, taking the sharpness of the pattern perceived through the specimen as a measure of its transparency. This is termed *contact transparency*. But full transparency (which is our ultimate goal) does not involve direct contact; consequently, we also examined the ceramics in terms of the more stringent property of *distance transparency*, with the specimens placed 1 cm above the back-lit pattern. In **Figure 11** we see how the temperature of hot pressing affects the transparency of the $SrHfO_3$:Ce ceramic specimens under the two different conditions of observation. Note that while the contact transparency hardly varies at all, there is a progressive loss of distance transparency with increasing hot press temperature.

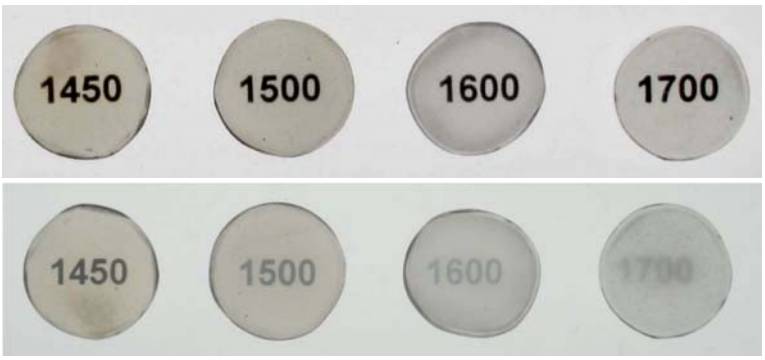

Figure 11. Transparency of specimens hot-pressed at the indicated temperatures (°C). Upper picture shows specimens in contact with text; lower, 1 cm above text.

Although the above gives us a qualitative indication of the transparency of $SrHfO_3$:Ce ceramics, it is not adequate to determine if a sample will transmit an image of a more distant object, such as would be perceived though a glass window. In order to obtain a quantitative measure of the transparency, we used a Stover scatterometer (**Figure 12**) to examine the extent to which a light beam is degraded, as function of angle from the incident beam, upon passing through the $SrHfO_3$:Ce ceramic specimen. The spectra (**Figure 13**) consist of two distinct features: a relatively low-level background that rises to a broad maximum centered at zero degrees, corresponding to light that has been scattered; and a tall sharp central peak generated by forward-propagated light that passes through the sample *without* being scattered. This is a fundamental distinction: while forward-scattered light can provide contact transparency, imaging of distant objects depends on light passing *unscattered* directly through the specimen*. Thus we

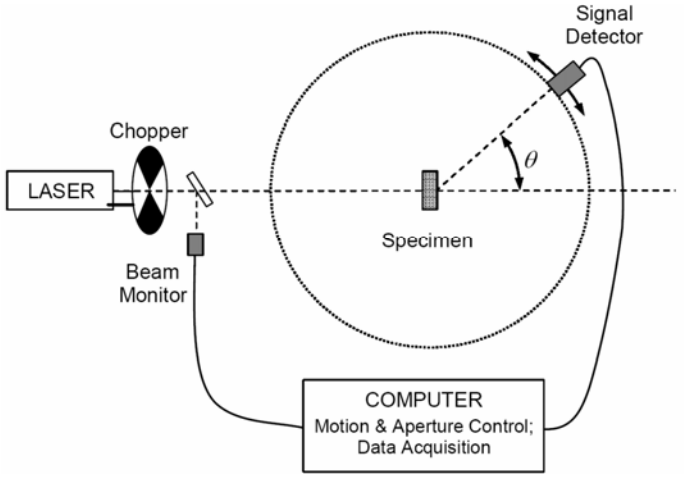

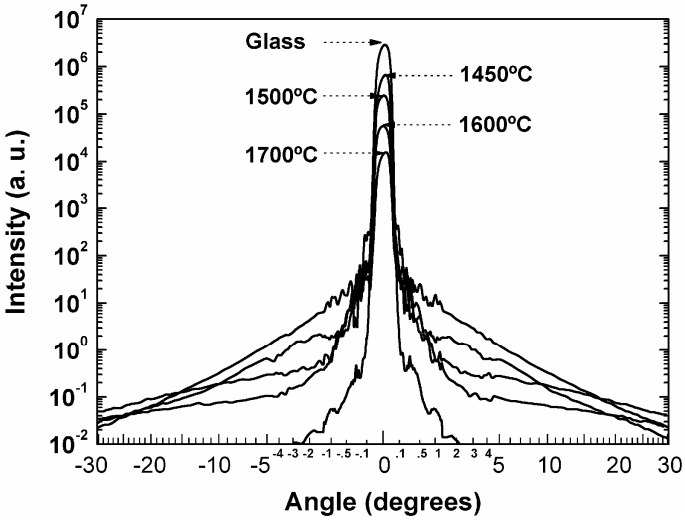

Figure 13. Scatterometer traces of the four $SrHfO_3$:Ce samples shown previously in **Figure 11,** hot-pressed at the indicated temperatures. The *y*-axis is logarithmic to accommodate the great dynamic range, while the *x*-axis is scaled as square root of angle so as to display a broad angular range without losing detail at small angles.

* This is why simple in-line transmission fails as criterion; it records all forward-propagated light, making no distinction for whether it has been scattered.

can quantify the true (remote) transparency of various specimens by means of the relative magnitudes of their central peaks.

The heights of the central peaks show a well-defined inverse relationship with the hot-press temperature. From 1450ºC up to 1700ºC, the transparency of the $SrHfO_3$:Ce samples decreases from 24.2% to 0.55% relative to that of glass. Thus, these measurements confirm that samples whose contact transparencies are virtually identical can differ widely when used for imaging remote objects (see **Figure 11**), and that to maximize the latter, hot-pressing of $SrHfO_3$:Ce should be done at the lowest possible temperature consistent with achieving full density.

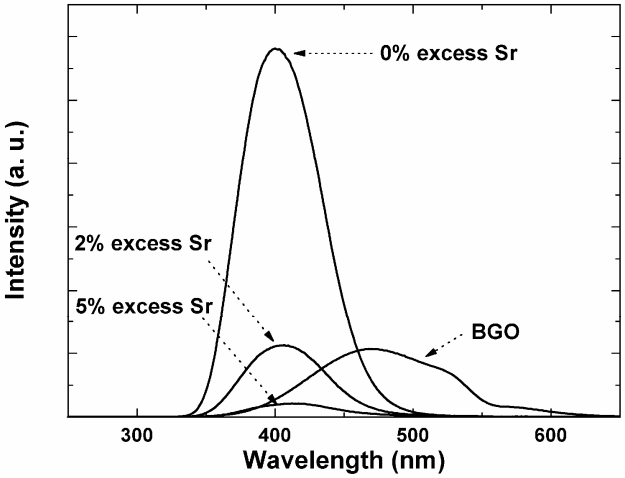

Figure 14. Radioluminescence spectra of $SrHfO_3$:Ce ceramics made from powders containing various concentrations of excess Sr.

3.4.5. Radioluminescence of the Ceramic

The radioluminescence of $SrHfO_3$:Ce ceramics is affected by many factors, both chemical and physical. The next two figures present two of these influences. **Figure 14** shows the effect of various concentrations of excess Sr in the initial powder batches. Also shown is the spectrum of a BGO crystal for comparison. The spectrum of $SrHfO_3$:Ce consist of a broad emission band in the near UV and visible violet spectral region, which is attributed to the *5d→4f* transition of Ce^{3+} [17]. The radioluminescence intensity of the $SrHfO_3$:Ce ceramics decreases dramatically with an increasing amount of excess Sr. To the extent that the hafnate lattice can accommodate this excess in solid solution, it would introduce a charge imbalance that could be redressed by the conversion of some of the Ce^{3+} activator to the nonradiative tetravalent state. While this is only speculative, it is consistent with the known chemistry of the corresponding strontium cerate ($SrCeO_3$), and would explain the observed luminescence decrease.

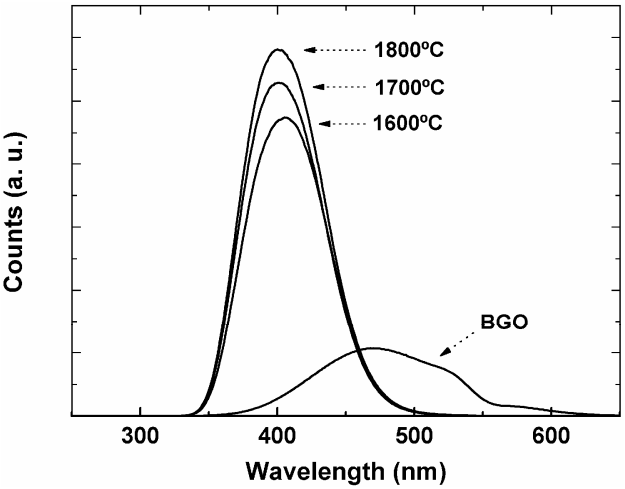

Figure 15. Radioluminescence spectra of stoichiometric $SrHfO_3$:Ce ceramics hot-pressed at various temperatures.

Figure 15 shows how the radioluminescence spectra of stoichiometric $SrHfO_3$:Ce ceramics (no excess Sr) are affected by the temperature at which the specimens were hot-pressed. Here we see that the luminescence intensity of the stoichiometric samples increases with hot-press temperature, although the range of variation is much smaller than in the previous case. Thus we are faced with a trend conflict, with optimal transparency at the lowest of the acceptable hot pressing temperatures, but optimal emission at the highest. Nevertheless even the worst of the three is substantially brighter than BGO, so that it may yet be feasible to reach an acceptable trade-off.

3.5. Evaluation of Sinter-HIPed Strontium Hafnate

The sinter-HIP approach to the fabrication of strontium hafnate ceramics became a feasible alternative to hot pressing only quite late in the program (essentially the last nine months), when nanopowders of the material became available from Nanocerox. Consequently, studies of the consolidation process and evaluation of the resulting specimens could not be conducted at quite as

comprehensive level as for the hot pressed material. Nevertheless, evidence thus far indicates that the technology has great promise, and work beyond the expiring SBIR program is continuing in-house as time and resources permit. The next two sections summarize the state of this effort.

3.5.1. Similarities with Hot-Pressed Material

It is reasonable to expect that once processes are optimized, the properties of fully dense transparent strontium hafnate ceramics should be independent of the manner by which they were fabricated. For many of the physical observables this is largely true. Certainly the issue of *Phase Fidelity* (**Section 3.4.2**) is as relevant with regard to sinter-HIPing as for hot pressing. Kinetics aside, the various phases themselves and the transitions between them are strictly material properties, and do not depend on processing conditions. We have not found these transitions to be a major impediment to the achievement of fully dense and transparent optical ceramics by means of hot pressing, and we have encountered no evidence to the contrary in the sinter-HIPing as well.

With regard to *Chemical Fidelity*, the same comments apply. In sinter-HIPing as with hot pressing the deliberate addition of extra SrO to forestall strontium loss during processing is deleterious to the radioluminescence (compare **Figures 16** and **14**). Moreover, the ultimate grain sizes are quite comparable (see **Figure 17**), although with sinter-HIPing the change-over from submicron to large grains appears to occur at somewhat lower temperatures. And, finally, sinter-HIPing has achieved a respectable level of contact transparency (see **Figure 18**), although a comparable level of distance transparency is yet to be reached.

3.5.2. Differences with Hot-Pressed Material

However, the sinter-HIP process still has quite a ways to go before it can reach the level already demonstrated by hot pressing. The latter has a two-year head start, and sinter-HIPing still has many more problems that remain to be resolved. Most notable of these (and clearly evident in **Figure 17**) is the abundant presence of an apparent glassy phase (or at least one that had been molten at sintering temperature). From EDS measurements (**Figure 19**) this anomalous phase appears to have a composition resembling that of the grain proper, but with a Hf:Sr

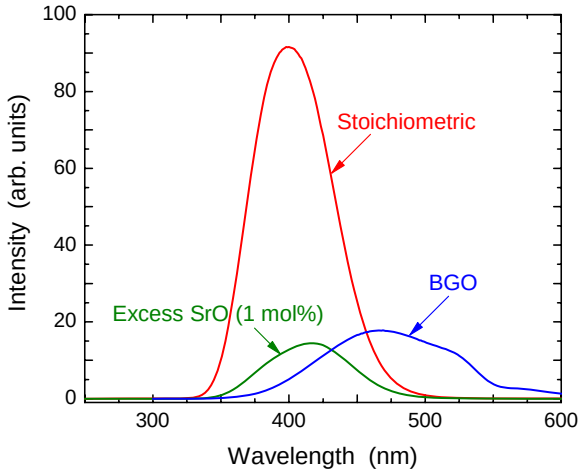

Figure 16. Radioluminescence spectra of sintered $SrHfO_3$:Ce disks made from powders with and without excess SrO.

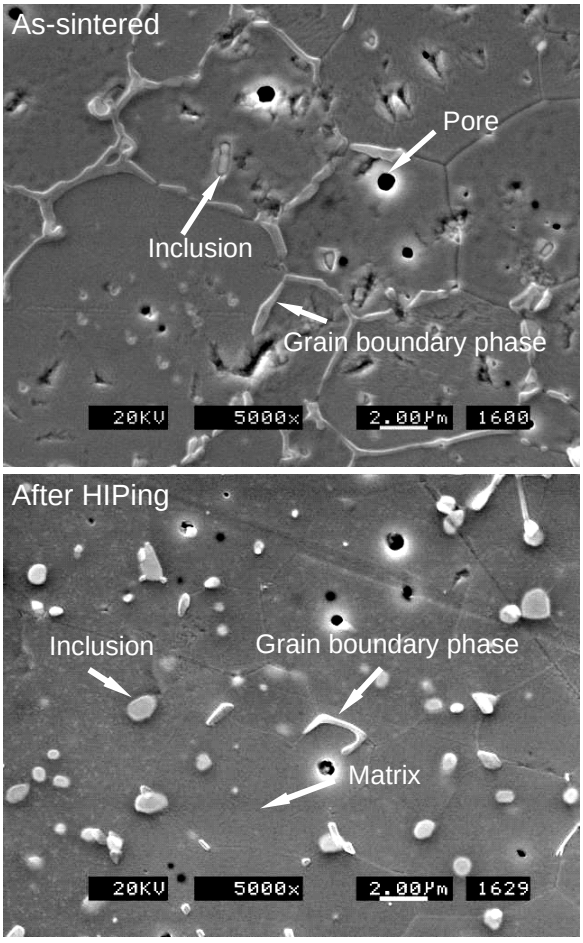

Figure 17. SEM micrograph of sinter-HIPed $SrHfO_3$:Ce disk, showing grain structure and residual inhomogeneities. Top picture shows sintered compact before HIPing; lower picture, after HIPing.

ratio some 75% higher. This phase is segregated at the grain boundaries and may well be playing a significant role in the growth of the grains. HIPing appears to remove most of this anomalous phase (again see **Figure 17**), but remnants persist. It is difficult to believe that these can be anything but deleterious. Indeed, the high incidence of all inhomogeneities (inclusions and pores along with the interfacial phases) makes the achievement of any transparency at all even more remarkable, and an indication of the potential of the sinter-HIP approach. Clearly, much further study is warranted.

Figure 18. Contact transparency of sinter-HIPed $SrHfO_3$:Ce disk in direct contact with back-lit text.

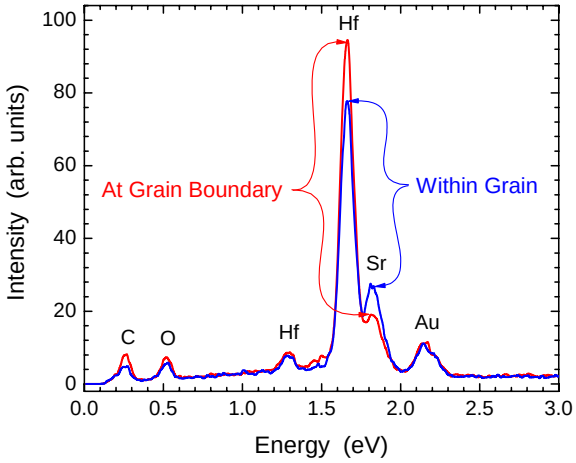

Figure 19. EDS spectrum of sintered $SrHfO_3$:Ce ceramic before HIPing (see **Figure 17**). Peak heights indicate that Hf:Sr ratio in grain boundary phase is ~75% greater than in grain proper.

4. CONCLUSION

We have studied the morphology, transparency, and optical properties of $SrHfO_3$:Ce ceramics. Ceramics can be made transparent by carefully controlling the stoichiometry of the precursor powders. When fully dense, transparent samples can be obtained. Ceramics with a composition close to stoichiometry (Sr:Hf ~ 1) appear to show good transparency and a reasonable light yield several times that of BGO. The *contact* and *distance* transparency of ceramics hot-pressed at about 1450ºC is very good, but deteriorates at increasingly higher hot-press temperatures. If these ceramics can be produced in large quantities and sizes, at low cost, they may be of considerable interest for PET and CT.

REFERENCES

1. http://www.orau.org/ria/
2. Knoll G, *Radiation Detection and Measurement*, 3rd Ed. (John Wiley and Sons, 1999).
3. Rodnyi PA, *Physical Processes in Inorganic Scintillators* (CRC Press, New York, 1997).
4. Moses WW, "Current Trends in Scintillator Detector Materials," *Nucl. Instr. & Meth. A* 487, 123 (2002).
5. Derenzo SE, Moses WW, "Experimental Efforts and Results in Finding New Heavy Scintillators," in *Heavy Scintillators*, DeNotaristefani F, Lecoq P, Schneegans M, editors (Editions Frontieres, 1993).
6. Mandal BP, Garg N, Sharma SM, Tyagi AK, "Preparation, XRD and Raman spectroscopic studies on new compounds $RE_2Hf_2O_7$ (RE = Dy, Ho, Er, Tm, Lu, Y): Pyrochlores or defect-fluorite?," *J. Solid State Chem.* 179, 1990 (2006).
7. Patil KC, Aruna ST, Mimani T, *Curr. Opin. Solid Mater. Sci.* 1, 507 (2003).
8. *Carbon Black: Science and Technology*, Donnet J-B, Bansal RC, Wang M-J, editors., (M. Dekker, New York, 1993).
9. Vemury S, Pratsinis SE, Kibbey L, *J. Mater. Res.* 12, 1031 (1997).
10. Laine RM, Bickmore CR, Treadwell D, K. Waldner K, U. S. Patent 5,958,361 (1999).
11. Sutorik AC, Paras MS, Lawrence D, Kennedy A, Hinklin T, *Ceram. Trans.* 147, 73 (2003)
12. Villanueva-Ibañez M, LeLuyer C, Parola S, Dujardin C, Mugnier J, "Influence of Sr/Hf ratio and annealing treatment on structural and scintillating properties of sol–gel Ce^{3+}-doped strontium hafnate powders," *Opt. Mat.* **27** (2005) 1541 – 1546.
13. Shevchenko AV, Lopato LM, Stegnii AI, Ruban AK, Dvernyakov VS, Pasnichnyi VV, *Inorganic Materials* **17** (1981) 741.

14. Kennedy BJ, and Howard CJ, "High-temperature phase transitions in $SrHfO_3$," *Phys. Rev. B* **60** 2972 – 2975 (1999).

15. Yamanaka S, Maekawa T, Muta H, Matsuda T, Kobayashi S, Kurosaki K, "Thermal and mechanical properties of $SrHfO_3$," *J. Alloy Comp*. **381** (2004) 295 – 300.

16. Loureiro SM, Gao Y, Venkataramani V, "Stability of Ce(III) Activator and Codopant Effect in $MHfO_3$ (M = Ba, Sr) Scintillators by XANES," *J. Am. Ceram. Soc*. **88** (2005) 219 – 221.

17. van Loef EV, Higgins WM, Glodo J, Brecher C, Lempicki A, Venkataramani V, Moses WW, Derenzo SE, and Shah KS, "Scintillation Properties of $SrHfO_3:Ce^{3+}$ and $BaHfO_3:Ce^{3+}$ Ceramics," *IEEE Nucl. Sci. Symp. Conf. Rec*., vol. 4, pp. 1538 – 1540 (2006).